DEPARTMENT OF AUTOMATIC CONTROL AND SYSTEMS ENGINEERING
THE UNIVERSITY OF SHEFFIELD

Electrodynamic simulation of inertia load

by

J.B. Edwards and R. J. Chidzonga
(Industrial Control Research Group, AC&SE)

AC&SE Research Report No. 555

Dated 6 January 1995

Electrodynamic Simulation of Inertia Load

Abstract: Dynamic response in most electromechanical motion control systems is dominated by the rate terms. The need to simulate load often arises in testing such systems or algorithms. This report addresses the issue of stability in dynamic inertia load simulation using coupled machines. A criterion limiting the simulated inertia is derived. No suitable scheme has however been identified to avoid violation of this stability criterion in trying to simulate arbitrarily large inertia load apart from recourse to DSP.

1 Introduction

Load models are essential in diverse situations in simulation studies. This report focuses on stability in inertia load simulation by dynamometry systems typified by Figure 1.0. This consists of a torque absorbing device coupled to a drive engine shaft directly or through a component under test thus producing an interactive engine-dynamometer system. A dc generator(G) and motor(M) respectively assume these roles in our case. The dynamometer's role is to subject the prime mover to characteristic simulated loads in testing the drive systems[1, 2] or verification of control algorithms[3, 4]. Particular descriptions of dynamometer types viz. regenerative and absorbing can be found in[4] and [5] respectively. In the literature most such systems operate under independent dynamometer or load control [6] especially when efficiency and power analysis are the principal interests.

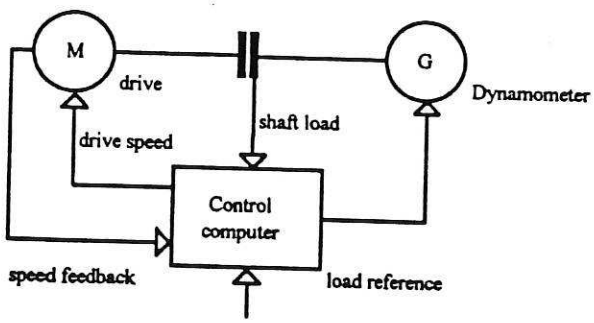

Figure 1.0 Load simulation system schematic, excludes intermediate power components.

In regenerative dynamometry the engine and dynamometer in addition to the mechanical coupling are also electrically coupled giving rise to two main control problems namely stability and interaction. In [2] Stringer achieved limited performance in using SISO classical stabilisation techniques for road load simulation using an arrangement similar to Figure 1.0 but under continuous time control. Edwards[7] models this configuration as 2×2 multivariable system and discusses drive-load de coupling control. When load calculation is entirely digital instability is reported and the ensuing analysis postulates a stability criterion limiting the inertia load that can be simulated. In[8, 9] using dedicated hardware no stability problems are reported in respect of this limit.

Inertia load is a pertinent problem in high accuracy electromechanical motion control and its simulation allows replacement of dead loads as used in[10] hence affords us more versatility. The inherent stability problem emanating from[7] does not feature in literature explored by this author and yet in its simplicity it is crucial to stable inertia simulation. We proceed to a formal statement of this problem and the assumptions made in the subsequent analysis. The terms prime mover, drive and engine are used inter-changeably.

Given a sampling frequency the condition postulated in[7] sets the upper stability limit of the inertia to be simulated as a trade in of three factors namely the sampling period, inertia of physical prime mover and the lag used in the speed signal prefilter. This report extends the analysis with the objective of attesting this criterion for the load loop under the same assumptions, i.e.

1- drive motor torque can be manipulated directly through tight armature current control.

2-dynamometer load torque can manipulated directly through tight armature current control.

These assumptions are justifiable under constant flux operation in view of the very small armature and power converter time constants, and stiff driver-load coupling. Under variable flux appropriate modifications should be made to take account of extra time lags. The underlying dynamics of the system can be investigated through these assumptions that allow the machines to behave ideally. Conclusions derived can then be re-appraised in the light of simulation results with realistic models.

The structure of the remainder of the report is as follows. A continuous and discrete model of Figure 1.0 based on the above assumptions are presented. These are slightly different to those used in[7]. Following this are numerical results showing that the postulated criterion though correct in form needs a correction factor to agree with simulation results. An analytical solution based on differential calculus is then outlined. This yields a criterion that agrees with the numerical and simulation results. Drive loop dynamics and a control strategy based on the Zero Phase Error Tracking Controller(ZEPTC)[11] are then discussed prior to presentation of simulation results for the coupled system.

2 Load loop model

With reference to Figure 1.0 define the following variables.

$T_m(t)$ drive torque developed by the motor, Nm.

$T_g(t)$ load torque developed by the generator, Nm.

$T_d(t)$ desired load torque (to be simulated), Nm.

$T_s(t)$ motor output torque, i.e. that available to drive mechanical load, Nm.

$T_e(t)$ error between dynamometer and desired load torque, Nm.

J_m, J_g drive and dynamometer inertia, Kgm^2.

J_v inertia to be simulated, Kgm^2.

k_2, ω dynamometer proportional constant and system speed, Nm/Nm and rad/sec.

A general load model can be formulated as an integral-differential equation(1). In vehicle systems for example $d\omega/dt$ would relate to mass or inertia, ω to aerodynamic, $\int \omega dt$ to position dependent and R constant loads.

$$T_d(t) = f\left(\omega, \frac{d\omega}{dt}, \int \omega dt\right) + R \tag{1}$$

The load of interest here concerns the mass and aerodynamic terms. Aerodynamic load is formulated as being proportional to speed through a quasi-constant λ(Nms/rad), justification is given later. Simple relationships relating these variables are given in equations (2) to (5) where the dynamometer loop is under unit feedback proportional control. $T_{er}(t)$ is a fictitious load error reference introduced for mathematical convenience. In practice it is zero. We drop the time variable 't' for simplicity.

$$T_s = T_m - (J_m + J_g) \cdot \frac{d\omega}{dt} \tag{2}$$

$$T_d = J_v \frac{d\omega}{dt} + \lambda\omega, \quad R = 0 \tag{3}$$

$$T_g = k_2 (T_{er} - T_e) \tag{4}$$

$$T_e = T_g - T_d \tag{5}$$

Manipulation of these equations gives the working block diagram in Figure 2.0. This is depicted as a two-by-two multivariable system to emphasise the presence of two interacting loops.

There are difficulties with sampling and differentiation that arise in inertia simulation. Acceleration sensors are not available [12] for implicit computation of (3). Noise complicates direct differentiation of speed or position signals. Higher orders differentiating filters, e.g. the Kalman filter based [13] introduce more lag which degrades tracking. The use of a simple prefilter in the speed loop inevitably results in loss of signal derivative information. In this application however this fact counts less since a zero order lag greatly compensates for the otherwise unstable system.

3 Stability limits of the dynamic loads

The approach adopted to establish simulation limits of dynamic inertia and aerodynamic load is to look at three simple cases in the load loop, namely

(i) $T_m = 0,\ J_v \neq 0,\ \lambda = 0$

(ii) $T_m = 0,\ J_v = 0,\ \lambda \neq 0$ and

(iii) $T_m = 0,\ J_v \neq 0,\ \lambda \neq 0$

Equations (6) to (8) derived from Figure 3.0 summarise the model of the general case(iii). The other two cases follow by appropriate substitutions in these expressions.

$$w^*(s) = \frac{(1-e^{-sT})}{s^2 J(sT_L+1)} \cdot (T_m^*(s) - T_g(s)) \tag{6}$$

$$T_d(z) = J_v\left(\frac{z-1}{Tz}\right)\omega(z) + \lambda\omega(z) \tag{7}$$

$$T_e^*(s) = T_g^*(s) - T_d^*(s) \tag{8}$$

$$T_g(s) = k_2 (T_{er}^*(s) - T_e^*(s)) \cdot (1-z^{-1})\frac{1}{s} \tag{9}$$

3.1 Inertia load $J_V \neq 0$ and $\lambda = 0$

We look at case(i) where T_m is regarded as fixed and hence of no dynamic interest. From the above equations the open loop transfer function(OLTF) governing the load error is derived as,

$$\frac{T_e}{T_{er}}(z) = \frac{k_2}{J} \cdot \frac{TJz^2 + (-aTJ + J_v(T_L(a-1)+T))z - J_v(aT + T_L(a-1))}{Tz(z-a)} \tag{10}$$

where,

$$a = e^{-T/T_L}$$

$$J = J_g + J_m. \tag{11}$$

Defining $c = J_v/J$, and $b = T/T_L$, the open loop zeros of the system are the quadratic solution of (12).

$$z^2 + [-a + c + \frac{(a-1)c}{b}]z - c[a + \frac{(a-1)}{b}] = 0 \tag{12}$$

If we further define the second, first and zero order coefficients in (12) as α_2, α_1, and α_0 respectively the solution to (12) becomes,

$$z = \frac{-\alpha_1 \pm \sqrt{\alpha_1^{\,2} - 4\alpha_0\alpha_2}}{2\alpha_2} \tag{13}$$

When sampling is fast, i.e. $b \Rightarrow 0$ it is easily shown by direct substitution that α_1 and '$-4\alpha_2\alpha_0$' in (13) approach indeterminant ratios. Numerically these ratios are approximated by '-a/2' and '-2bc' respectively. As shown later an analytical derivation of these limiting values is possible through l'Hospital rule.

In Figure 5.0a the plots above and below show the exact α_1, $-4\alpha_2\alpha_0$ respectively plotted against b. In each case they include the approximations suggested earlier and '-a' and '-4bc' in[7]. The parameter 'c' or inertia ratio is put to its stability limit '1/b' according to[7]. The plots above show that '-a/2' is closer to α_1 than '-a' equally from plots below '-2bc' is closer to $-4\alpha_2\alpha_0$ than '-4bc'. For the particular case cb=1 these graphs prove that the postulations of [7] need a correction factor of 1/2 respectively over the interval of interest where the sampling frequency varies from theoretically infinity to 5 Hz, T_L being assumed to be one time units. Following this we show how we generalise approximations suggested here leading to a more precise boundedness criterion for the load loop dynamic response.

3.2 Simulated inertia upper bound

The analytical derivation of the upper bound of simulated inertia proceeds from open loop zeros in(12) and is inspired by the stability condition c≤1/b[7]. Suppose we are given a positive number ε such that

$$\|\varepsilon\| \le M, \text{ where } M \ge 0. \tag{14}$$

If 'c' is selected according to $c = \varepsilon/b$ where M = 1 corresponds to the critical case[7] then α_1 and '$4\alpha_1\alpha_0$' in (13) become explicit functions of 'b' $f_1(b)$ and $f_2(b)$ respectively given below.

$$f_1(b) = \frac{\varepsilon(b-1) + e^{-b}(\varepsilon - b^2)}{b^2} \tag{15}$$

$$f_2(b) = 4\varepsilon \cdot \frac{(1+b)e^{-b} - 1}{b^2} \tag{16}$$

When $b \Rightarrow 0$ both numerators and denominators of $f_1(b)$ and $f_2(b)$ approach zero giving rise to a pair of indeterminant ratios. For our particular case the limiting values of $f_1(b)$ and $f_2(b)$ according to [14] can be obtained from expression (17) where *h(b)* and *g(b)* are the appropriate numerator and denominator functions. The resulting limits are given in expressions (18) and (19).

$$\lim_{b\to 0} f_i(b) = \frac{h''(b)}{g''(b)}, \quad h''(b) \text{ is the second derivative wrt. b} \tag{17}$$

$$f_1(b) = \frac{(-2+\varepsilon)a}{2}\Big|_{b\to 0} \tag{18}$$

$$f_2(b) = -\frac{4b\varepsilon e^{-b}}{2b} \approx -2bc\Big|_{b\to 0} \tag{19}$$

A choice of ε = 1 leads to numerical approximations given earlier. Figure 5.0b is a similar comparison as Figure 5.0a. It uses the analytic approximations for ε = 0.5. The accuracy is consistent. From equations (18), (19) and (13) OLTF zeros become,

$$z = \frac{-(\varepsilon/2-1)a \pm \sqrt{(\varepsilon/2-1)^2 a^2 - 2bc}}{2}. \tag{20}$$

It is important to note that (18) and (19) are independent of ε only 'b' is restricted. The practical domain where these simplifications are applicable to within 8% error is $0 \le b \le 0.1$. Due to $T_{er} \equiv 0$ the obvious option available to control the load loop is feedback. In other words k_2, should be large to zero the load error fast. In turn this implies confinement of open loop zeros within the z-plane unit circle for closed loop stability i.e.,

$$\left|\frac{-(\varepsilon/2-1)a \pm \sqrt{(\varepsilon/2-1)^2 a^2 - 2bc}}{2}\right| \le 1.0. \tag{21}$$

Of the three classical cases arising out of this requirement the most important is the one when the zeros are complex or $(\varepsilon/2-1)^2 a^2 - 2bc < 0$ giving,

$$\left|\frac{-(\varepsilon/2-1)a \pm j\sqrt{2bc-(\varepsilon/2-1)^2 a^2}}{2}\right| \le 1.0 \quad \text{or} \quad cb \le 2 \quad \text{or} \tag{22}$$

$$\frac{J_v}{J} \le \frac{2T_L}{T}, \qquad k_2 >> 1.0 \tag{23}$$

The two cases corresponding to the discriminant being zero and positive give stable zeros. This is easily shown by considering the zeros in (22) to be going real through the discriminant changing from negative to zero then positive. The theoretical maximum of real roots correspond to c=0 and occur at z =a and 0. For any 'c' below the critical value in (22) the zeros thus remain stable. We can concluded from this analysis that inequality (23) sets the upper stability limit of the inertia ratio 'c' given the sampling period T and the lag compensator time constant T_L.

3.3 Combined dynamics of aerodynamic and inertia load

The aerodynamic load component is actually proportional to ω^2 [15]. Over a small speed range a conservative linear estimate can be made through the quasi-constant λ and hence the expression (3). The resulting open loop transfer function for $J_v \neq 0, \lambda \neq 0$ is not easily amendable to general analytic solutions. By linearity J_v can be set to zero and the dynamics investigated for aerodynamic load only. This results in the OLTF of equation(24).

$$\frac{T_e}{T_{er}}(z) = k_2 \cdot \frac{z^2 + (a_1\lambda / J - (a+1))z + (a + a_0\lambda / J)}{(z-1)(z-a)}, \text{ where} \qquad (24)$$

$$a_1 = T_L(b + a - 1), \quad a_0 = -T_L(ab + a - 1)$$

Closed loop input-output boundedness is ensured by satisfying the condition $|k_2 + 1| > |a + k_2(a + \lambda a_0 / J)|$ [16] which upon manipulation using the second order binomial series approximation for 'a' gives a stability criterion(25),

$$\lambda < \frac{2J}{T} \text{ or } \tau_1 > \frac{T}{2}, \qquad k_2 >> 1 \qquad (25)$$

$$a = e^{-b} \approx 1 - b + \frac{b^2}{2}, \qquad b << 1$$

τ_1 is a time constant defined as J/λ. In practice the balance between J and λ[17] ensures that this condition is satisfied. Figure 6.0 shows the error behaviour for λ=5, 15 and 50 Nm/rad/sec. It is oscillatory reflecting the interactive effect of the drive on the load loop characterised by (26). The dumping coefficient ζ and natural frequency ω_n are derived from an equivalent continuous model and k is loop gain of the drive. When J_V is no-longer zero frequency response techniques show that closed loop dynamics for cases (ii) and (iii) differ slightly as long as (25) is satisfied.

$$\frac{T_{\sigma}}{\omega}(z)=\frac{-\lambda}{k_2+1},\quad \omega_n^2=\frac{\lambda+k}{JT_L},\quad \varsigma=1/2\sqrt{\frac{J}{T_L(\lambda+k)}} \tag{26}$$

Figure 7.0 is a bode magnitude and phase plot for J_v=250 Kgm^2 and λ taking four values from 0 to 250 Nm/rad/sec. For each λ these plots confirm the statement earlier about the cases (ii) and (iii). The nyquist frequency and phase margin remain substantially unaltered.

4 Drive loop dynamics

The assumption of a tightly controlled armature current made at the beginning of this report allows the dynamics of the drive motor to be described by a torque constant k_1(Nm/A). This results in the driver block diagram in Figure 3.0. D(z) is a discrete speed compensator and $\omega_r(k)$ the reference speed profile to be tracked. The discrete OLTF(27) can be obtained from(6) by setting $T_g=0$ and $T_m=k_2k_cD(z)(\omega_r(z)-\omega(z))$. k_c is the power converter gain.

$$\frac{\omega}{\omega_r}(z)=k\cdot\frac{a_1z+a_0}{J(z-1)(z-a)} \quad \text{where } D(z)=k_s, k=k_1k_ck_s \tag{27}$$

The root locus of the closed loop characteristic equation is a circle of centre $(-a_0/a_1,0)$ and radius r given by(28). For b<<1 the centre approaches (b-1, 0) and the radius $2\sqrt{1-b}$. As in(25) we can also show that drive loop gain is limited according to estimate(29). Simulations show that feedback compensation, e.g. a PD controller drastically reduces the limit on simulated inertia hence undesirable.

$$r^2=\left(\frac{a_0}{a_1}\right)^2+\left(\frac{a_0}{a_1}\right)(a+1)+a \tag{28}$$

$$k<\frac{2J}{T} \tag{29}$$

$$\frac{\omega}{\omega_r}(z)\Rightarrow\frac{kG_1(z)}{1+(k_2/(k_2+1))\cdot G_1(z)G_2(z)} \tag{30}$$

Due to interaction the load loop modifies the drive OLTF from (27) or $G_1(z)$ to (30) where $G_2(z)$ is the transfer function corresponding to (7). When $J_v=0,\lambda\neq 0$ (29) changes to $k+\lambda<2J/T$ and when $J_v\neq 0,\lambda\neq 0$ transient response improves subject to established conditions. Tracking performance was improved by disturbance compensation and feedforward control using the ZPETC referred to earlier. These strategies unlike feedback do not alter(23). Simulation results of the coupled systems are discussed in the following section.

5 Simulation results

For the idealised case considered in this report T_{er} was set to zero and the system perturbed by T_m the drive torque. The results are shown in Figures 8.0 to 11.0 in which parameters T, J_v and λ were varied to test predictions based on boundedness criterion derived earlier. For the coupled closed loop system results were obtained for a 30 second trapezoid cycle.

Figure 8.0a shows the step response for inertia at the stability limit of [7]. In Figure 8.0b the inertia load is 40% above this limit. Either responses are stable. The settling time increases for larger J_v. In Figure 9.0a, J_v is put to the limit in inequality (23). An optimised or judicious choice of gain can secure acceptable response and for larger gains as predicted oscillations break-up. In line with(23) a 30% increase in sampling frequency improves the response to Figure 9.0b.

Figure 10.0a compares the tracking response at the two definitions of critical inertia when $\omega_r(t)$ is trapezoid. The desired load T_d is fed-forward to compensate for T_g thus reducing tracking delay. Figure 10.0b is an exploded view of the speed profiles in Figure 10.0a. In Figure 11.0 tracking is compared for cases (ii) and (iii) when λ=15 Nm/rad/s and J_v=250 Kgm^2. The effect of the inertia load is seen to improve the transient dynamics. The power demand is however unlikely in practice since most inputs are smooth unlike the discontinuous step signal. For arbitrary inputs the inertia component reinforces stability of the aerodynamic component '$\lambda\omega$' as in Figure 11.0b.

These simulation results for the load loop and coupled system confirm that within the confines of the assumptions made in respect of the motor and generator the stability criterion(23) relating the ratio of inertia to sampling frequency and lag time dictates the dynamics of the system over $0 < b \leq 0.1$ and $k_2 >> 1.0$. Transient response degrades for larger J_v.

6 Discussion and conclusion

Current developments in dynamometry systems are tending towards small inertia[1, 18, 19] for low vibration noise and wide bandwidth response. Dispensing with unnecessarily large flywheels in simulations systems of the type discussed in this report then calls for higher sampling rates. Application of DSP addresses this issue in real time control. Notwithstanding they is always the attendant problem with unstable zeros in discrete systems introduced by fast sampling for systems of order greater than two[20]. The criteria thus derived provides a useful guide when performance improvements are sought in testing algorithms or equipment using simulated inertia.

Satoshi[9] models the load as in(1) and demonstrates higher performance of servo control based on acceleration or essentially inertia load compensation. Electric inertia simulation is also suggested by Sazuki[20] for related work. The drive for electric vehicle development is well under way for pollution control reasons. They is as a result renewed interest in the area of dynamic load simulation[18, 19] as possible new control strategies and drive systems are tested for implementation in the 'green' vehicles of tomorrow.

The analysis in this report has shown the limit placed on inertia simulation. At the present no alternative digital differentiating or filtering technique has been identified to overcome this limitation. In addition to finding a solution to this problem the analysis and conclusions drawn in this report will be extended to explore applicability of conclusions drawn to realistic models. This will also include consideration of non-stationary J_v and λ. Control and configuration of the drive and dynamometer will be considered to justify the assumptions made on direct manipulation of torque. Whiles use has been made of ideal models the results so derived expose the underlying dynamics providing useful insights into experimental design. Benefits to be derived from simulating inertia lie in versatility e.g. practical simplicity of subjecting systems under test to variant inertia load as happens e.g., in robot manipulators.

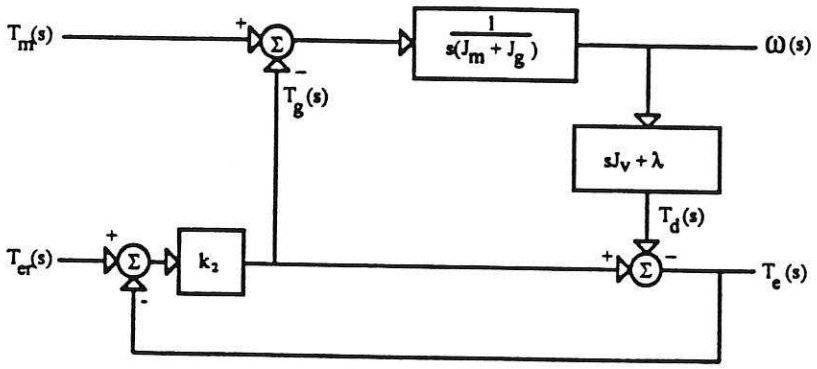

Figure 2.0 Basic model of dynamic load simulator , driver loop is open

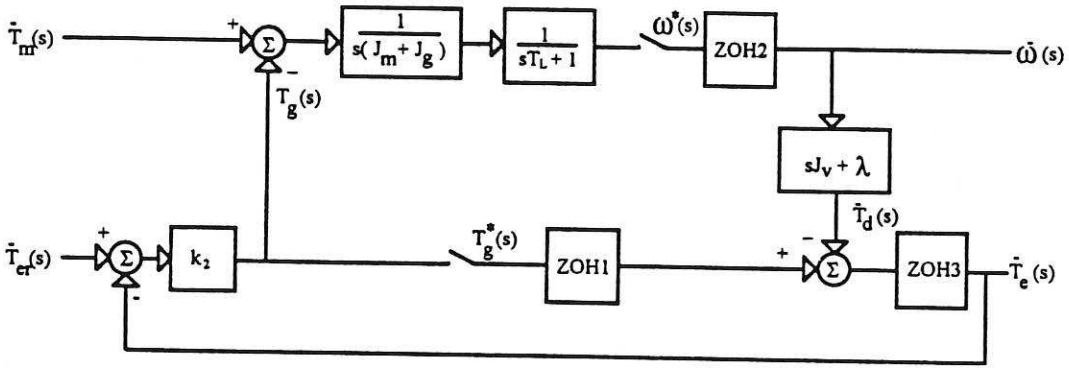

Figure 3.0 Equivalent discrete model of load simulator

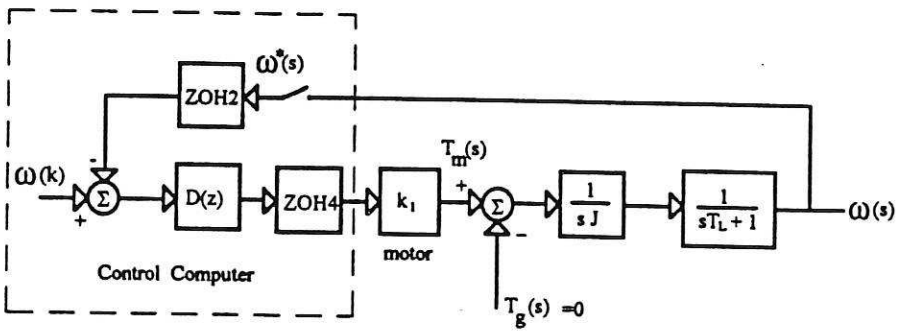

Figure 4.0 De-coupled drive model of load simulator

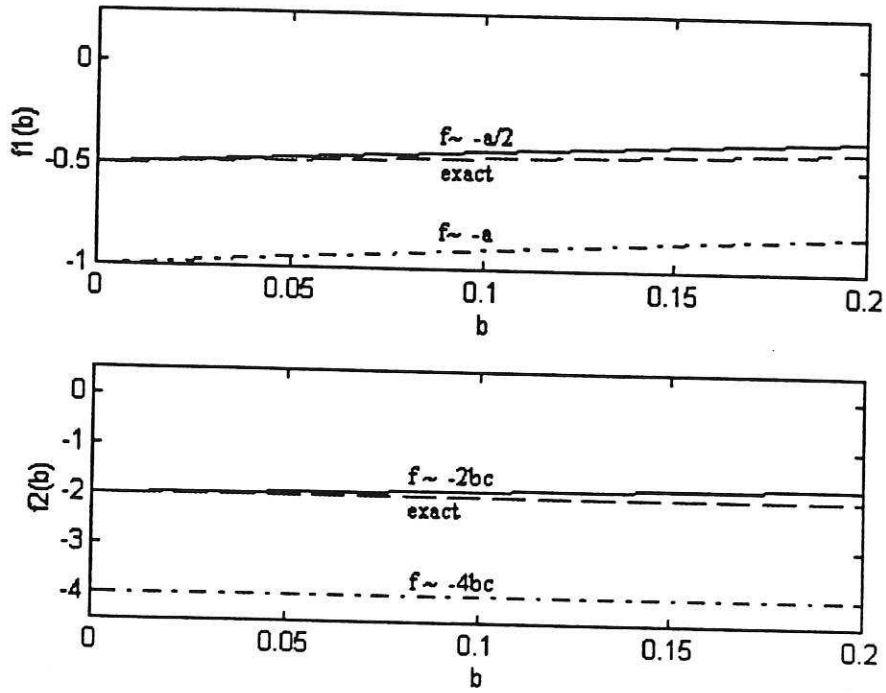

Figure 5.0a Numerical approximation of $f_1(b) and f_2(b)$ for cb=1.0

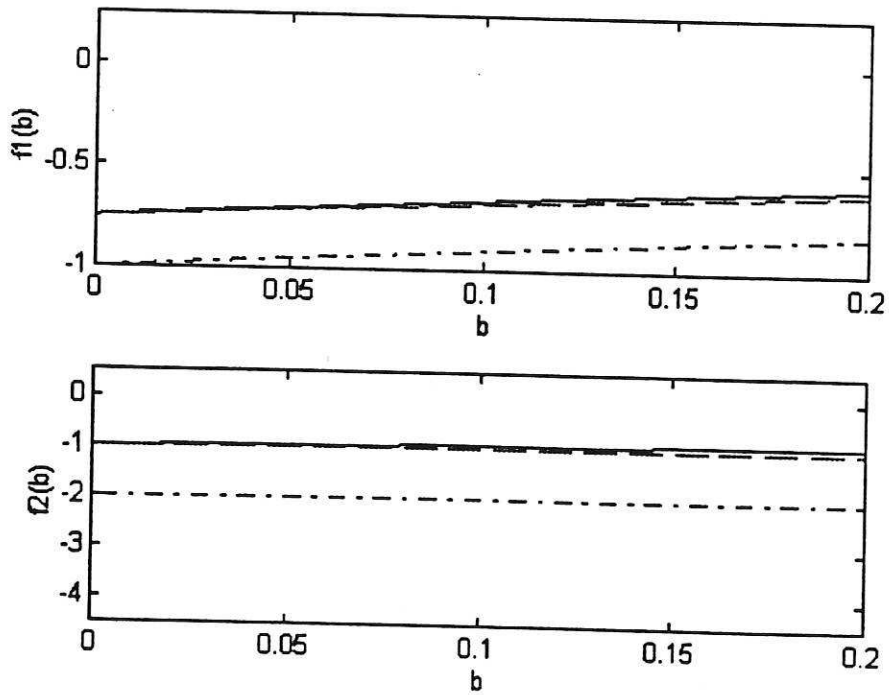

Figure 5.0b Analytical approximation of $f_1(b) and f_2(b)$ for cb=0.5

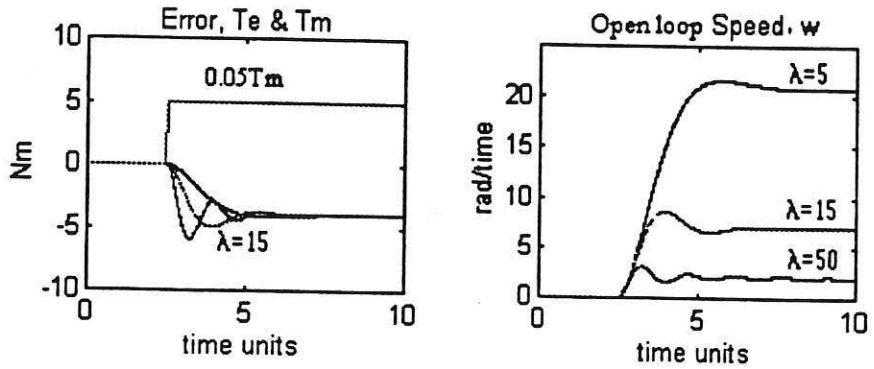

Figure 6.0 Load loop response to aerodynamic load for λ=5, 15 and 50.

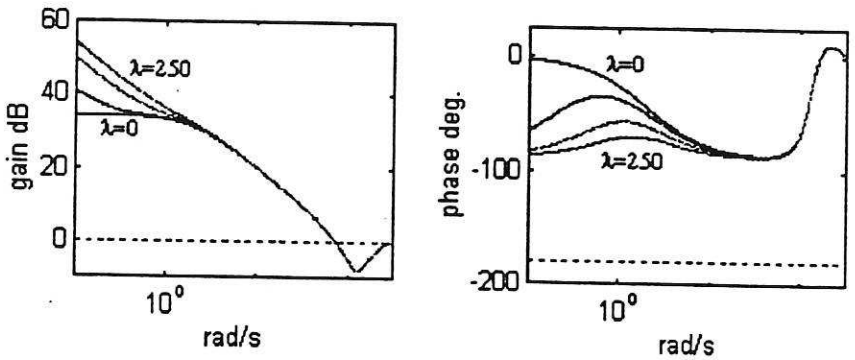

Figure 7.0 Open loop bode plots of load loop for combined inertia and aerodynamic load. λ takes on values 0, 50, 150 and 250 Nms/rad

Parameters: $k_2 = 25, T_L = 0.5, T = 0.01, J_g = J_m = 2.5, J_v = 250 Kgm^2$

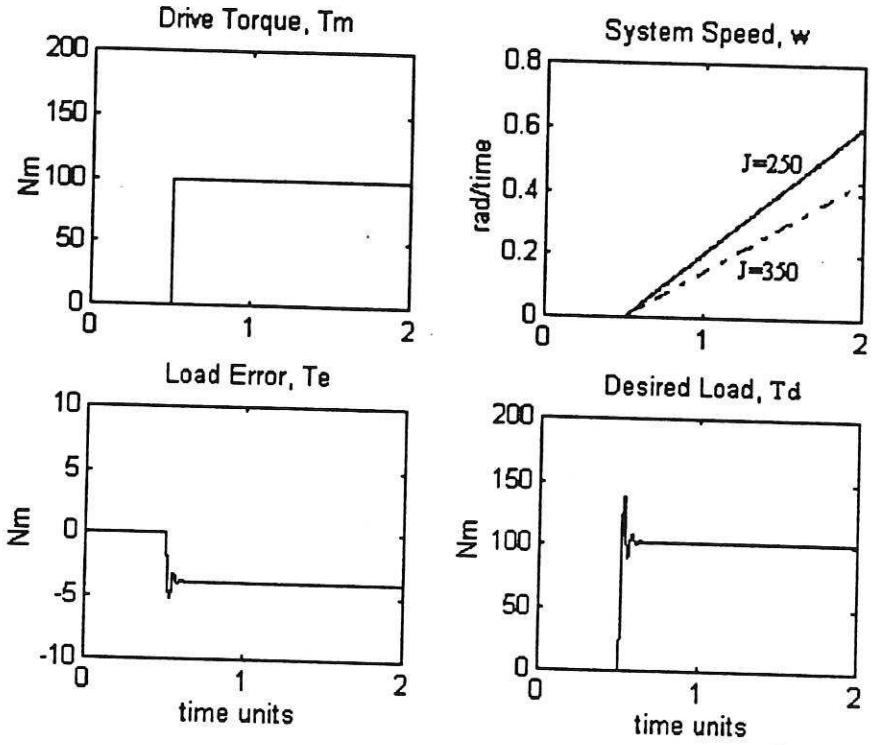

(a)

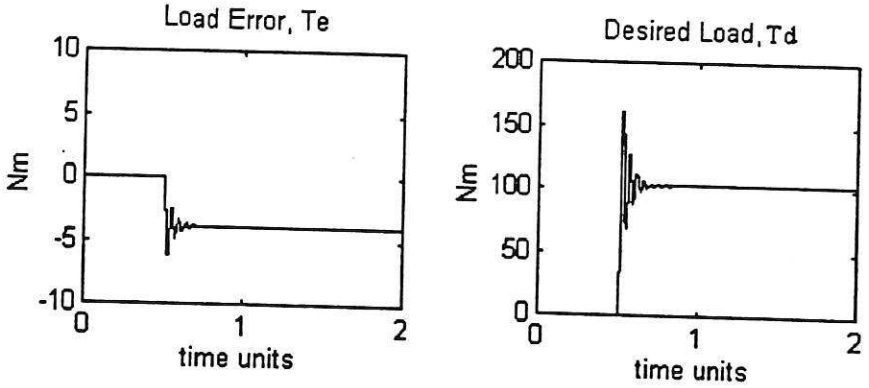

(b)

Figure 8.0 Step response of load loop $k_2 = 25, T_L = 0.5, T = 0.01, J_g = J_m = 2.5 Kgm^2$.
(a) simulated inertia is 250 and (b) 350 Kgm2.